https://doi.org/10.5194/egusphere-2026-4256
Preprint. Discussion started: 19 August 2026

Regime-dependent evolution of water vapor, cloud liquid, and cloud base before rain onset in the southeastern Alpine forelands

Esmail Ghaemi[1,2], Andreas Kvas[2], Ulrich Foelsche[1,2], and Pavlos Kollias[3,4]

[1]Institute of Physics, Department of Astrophysics and Geophysics (AGP), NAWI Graz, University of Graz, Austria
[2]Wegener Center for Climate and Global Change (WEGC), University of Graz, Austria
[3]School of Marine and Atmospheric Sciences, Stony Brook University, Stony Brook, NY, USA
[4]Environmental Science and Technologies Department, Brookhaven National Lab, Upton, NY, USA

Correspondence: Esmail Ghaemi (esmail.ghaemi@uni-graz.at)

Abstract. Liquid water path (LWP) and integrated water vapor (IWV) provide essential information on the moisture supply and condensation available for precipitation formation, while cloud base height (CBH) indicates where saturation and cloud formation start. The main goal of this study is to quantify how these parameters evolve before rain occurs.

We analyzed approximately 4 years of collocated observations from the WegenerNet 3D Open-Air Laboratory in southeast Austria, including an X-band dual-polarization radar, microwave and infrared radiometers, a GNSS station, and rain gauges. We separated convective and non-convective rain with a multi-criteria scheme based on radar polarimetric variables and the radiometer temperature profile, and warm, cold, and mixed rain types by comparing the echo top height with the -5 °C isotherm. During the six hours before onset, LWP stays low and then increases sharply within the last hour, with the steepest rise before convective events (about 300 g m^{-2}), while cold-season events show a more gradual increase of about 150 g m^{-2}. IWV changes earlier than LWP and is lowest in the cold rain type in both regimes. The joint evolution shows that convective events first move towards higher IWV and then towards a strong LWP increase near onset, while both parameters increase together in non-convective events. CBH decreases in all categories, most sharply before convective events (1000 m) and more modestly in the cold season (300 m). Overall, these signatures can serve as a reference to evaluate how models represent the transition from moisture to cloud and rain.

1 Introduction

Clouds and precipitation are important components of the Earth atmosphere and water cycle, influencing the atmospheric energy balance, freshwater availability, weather and climate processes, and a wide range of societal activities (Bony et al., 2015; Skofronick-Jackson et al., 2017). Although there have been many studies to understand the related processes through observation and modeling, the uncertainties in these observations, which can propagate into models, are still not fully understood (Stevens and Bony, 2013; Morrison et al., 2020). One of the important reasons is that cloud microphysical processes often occur on very small spatial and temporal scales. Liquid water path (LWP) and vertically integrated water vapor (IWV) are among these parameters and represent the total amount of liquid water and water vapor in a column of air, respectively. Although there is no direct way to measure LWP and IWV, there are several algorithms that retrieve them using various remote

https://doi.org/10.5194/egusphere-2026-4256
Preprint. Discussion started: 19 August 2026

sensing platforms, such as ground-based radiometers and satellite sensors (Billault-Roux and Berne, 2021; Kim et al., 2020). In addition to LWP and IWV which represent column-integrated liquid and vapor amounts, cloud base height (CBH) is closely related to the lifting condensation level for convective clouds and provides information on the thermodynamic level where saturation and cloud formation occur. Therefore, CBH adds an important context for interpreting cloud vertical structure and precipitation-related processes (Wallace and Hobbs, 2006). Both LWP and IWV can be retrieved using brightness temperature (T_b) from microwave radiometers by inverting, explicitly or implicitly, the radiative transfer through the atmospheric column. Infrared radiometers can estimate cloud-base height by associating the cloud-base brightness temperature to the corresponding altitude in a vertical atmospheric temperature profile (Wang et al., 2018).

Several studies focused on different atmospheric parameters, including the liquid water and integrated water vapor and their changes in course of precipitation. Wang and Hocke (2022) examined rainfall precursors over Bern, Switzerland, using 10 years of ground-based microwave radiometer observations, together with local weather-station data, covering 1199 rain events from 2011 to 2020. Their composite-analysis approach aligned rain events by onset time and examined eight atmospheric parameters before, during, and after precipitation. They found that at the onset of the event, IWV reached a peak and integrated liquid water rose rapidly in a short time. Before rain, infrared brightness temperature, IWV and wind speed showed a steep rise. Temperature reached a maximum about 30–60 min before rainfall while pressure and relative humidity reached minima within this time-frame. Over the Feldbach area in southeastern Austria, Haas et al. (2025) studied pre-rain conditions for convective events from 2020 to 2024. Using rain gauge data, warm-season precipitation events based on maximum precipitation rates above the 90th percentile were selected. Then, the authors examined the median evolution from 8 h before event onset to 16 h after event end for different parameters including IWV, LWP, cloud-base height, and absolute humidity. They found that IWV anomaly, LWP, and wind speed increased before onset, while cloud-base height decreased, indicating the arrival of convective systems. Additionally, spatial variability in precipitation, temperature, LWP, and cloud cover increased during rainfall, highlighting the localized nature of these heavy convective events. Building on the study by Haas et al. (2025), we extend the analysis in three ways. First, we included both convective and non-convective events, separate them using a radar-based convective probability metric. Second, we divide the events based on the location of the echo top and -5 °C isotherm. Lastly, we include events in cold months. With the event separation into different regimes and rain types, we want to differentiate formation pathways (shallow versus deep convection) in LWP and IWV. More precisely, we will investigate the following questions:

- How do LWP and IWV, together with CBH, change before convective compared to non-convective events?
- Does this evolution differ between shallow and deep convection?
- Are changes in LWP and IWV (liquid versus moisture building up) consistent across different regimes and types?

Additionally, we describe the monthly variability of LWP and IWV in rainy and non-rainy clouds, and present case studies to complement the long term analysis. The study is based on approximately four years of data (April 2021 – September 2025) from a microwave radiometer, an infrared cloud-base radiometer, a GNSS station, an X-band dual-polarization radar, and a climate station network.

https://doi.org/10.5194/egusphere-2026-4256
Preprint. Discussion started: 19 August 2026

The paper is structured as follows: The study area and data that are used are described in Sect.2. We present a detailed methodology including the rain type and regime classification in Sect.3. The results are shown and discussed in Sect.4, and finally, our conclusion is in Sect.5.

2 Study area and data

The study area is located in the southeastern Alpine forelands of Austria with moderate topography and altitude ranges of 250 m to 609 m. The region is characterized by hot summers and cold winters, and heavy rain from thunderstorms is dominant during summer (Kirchengast et al., 2014). The Mediterranean low pressure systems (Vb) affect the region as well, transporting humid mass and often cause major floods (Schröer and Kirchengast, 2018; Nissen et al., 2013; Kaitna et al., 2025).

As a long-term weather and climate monitoring facility, the WegenerNet climate station network has been measuring different meteorological parameters using 156 systematically distributed (e.g. 1 station in about 2 km^2) meteorological stations since 2007 near the town of Feldbach (46° 57' N, 15° 53' E), Austria (Fuchsberger et al., 2021; Kirchengast et al., 2014). In 2020, the WegenerNet station network was extended with the WegenerNet 3D Observing System, which features the following instrumentation: a dual polarization X-band radar, a six-station Global Navigation Satellite System (GNSS) network, a broadband infrared cloud structure radiometer, and a combined microwave/infrared tropospheric sounding radiometer. The combination of these instruments with the 156 existing ground stations forms the WegenerNet 3D Open-Air Laboratory for Climate Change Research and provides comprehensive atmospheric observations from the surface to the upper troposphere (Kvas et al., 2026).

In this study, we use data from the X-band radar, the microwave radiometer, the broadband infrared radiometer, a GNSS station, and a climate station, with the latter four instruments being collocated at the central station Raabtal (Fig. 1). We further use the average of four neighbouring rain gauges to identify precipitation events in combination with 2-m air temperature recorded at the radiometer location. We specifically use these local precipitation and temperature measurements, to only select precipitation events that ocurred at the radiometer site. The instrument data is processed by the WegenerNet 3D Processing System (Kvas et al., 2026), which features comprehensive quality control, to ensure robust retrievals of the physical atmospheric parameters. We make use of Version 1.0 L1b and L2 X-band radar data (Kvas et al., 2024a, b), and Version 2.0-rc1 L2a microwave and infrared radiometer data and GNSS station data (https://doi.org/10.5281/zenodo.21350494/, last access 14 July 2026).

3 Methodology

As a robust method for retrieval, microwave radiometers retrieve IWV mainly from channels near the 22.235 GHz water vapor absorption line, while LWP is retrieved from the combined response of water vapor and window channels, often including a channel near 31 GHz that is sensitive to cloud liquid water emission (Billault-Roux and Berne, 2021; Walbröl et al., 2022). In practice, retrievals require either statistical mappings, such as regression or neural-network algorithms, or physical/iterative

https://doi.org/10.5194/egusphere-2026-4256
Preprint. Discussion started: 19 August 2026

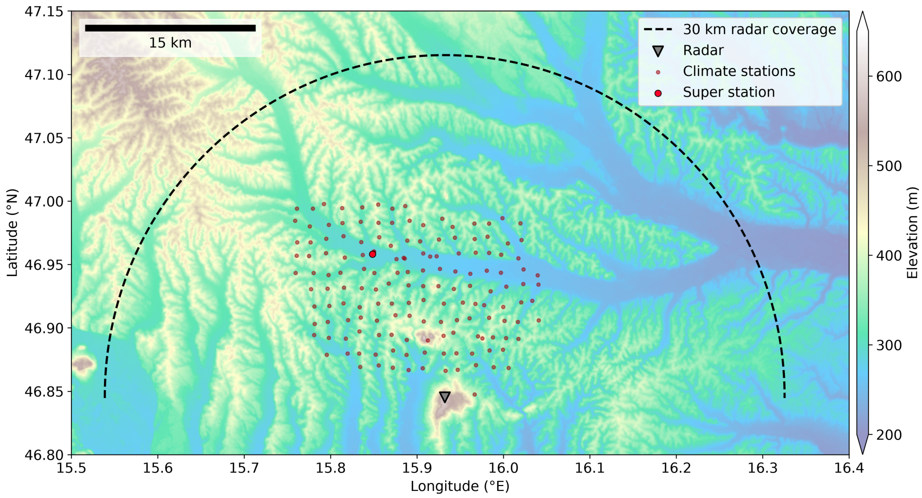

(a) An overview of the study area

(b) All instruments at the central station Raabtal (Super station)

Figure 1. An overview of the study area (top) and the instruments located at the central station Raabtal (bottom).

https://doi.org/10.5194/egusphere-2026-4256
Preprint. Discussion started: 19 August 2026

Table 1. Summary of the instruments which are used in this study

Instrument	Variables	Temporal resolution
Microwave radiometer	LWP and IWV	2.5 min
GNSS station	IWV	2.5 min
Infrared radiometer	CBH	2.5 min
Dual-pol X-band radar	Z_{h}, Z_{DR}, K_{DP}, v_{rad}, w_{rad}, ρ_{hv}	2.5 min
Rain gauge	precipitation	5 min

inversion methods based on a radiative-transfer forward model (Billault-Roux and Berne, 2021). Because IWV and LWP are retrieved indirectly, uncertainties arise from various sources such as instrument calibration, absorption models, and contamination by drizzle, rain, or wet-radome effects (Cadeddu et al., 2017). Although different methods have been developed to improve retrievals in cloudy scenes, the retrieval in precipitation remains a major source of uncertainty (Billault-Roux and Berne, 2021; Walbröl et al., 2022).

The signals received by a GNSS ground receiver are delayed by atmospheric water vapor among other effects. This delay is typically parameterized in terms of zenith wet delay (ZWD) and tropospheric gradients using a mapping function (Niell, 1996). The resulting ZWD estimates are converted to IWV using a weighted average temperature of the atmosphere (Bevis et al., 1992) which is forward modelled from surface measurements. The LWP and IWV from the microwave radiometer are retrieved from measured brightness temperatures using a neural network algorithm, which is tuned to the instruments location (Böck et al., 2025).

We filter the LWP and IWV data that are not flagged by quality control, which are not derived from interpolation (Kvas et al., 2026). This excludes time steps which the LWP retrieval has a large uncertainty (e.g. during precipitation). Then, we select cloudy time-steps using a minimum LWP of 10 g m^{-2}. This threshold is chosen as a conservative threshold to exclude noise and clear sky conditions, and has been used in previous studies (e.g. (Xi et al., 2022; Kiszler et al., 2023)).

To identify precipitation events, we apply a precipitation intensity threshold of 0.1 mm h^{-1}. A precipitation event occurred where this threshold is exceeded in at least 3 continuous time steps (equivalent to 15 min). Note that, to have the precipitation intensity in mm h^{-1}, we multiply the 5-minute data with 12. Then, if there were two consecutive events within 2 h, we merge them into one event. Snow events were filtered out by excluding precipitation events where the 2-m air temperature at the climate station was below 2 °C.

To classify events into warm rain, cold rain, and mixed rain, the following steps are taken:

1. Derive echo top values for each event, where the maximum height of non-zero reflectivity is located (from 1 h before until 1 h after the event initiation)

2. Calculate the spatial median, 90th percentile (P90), within a radius of 6 km around the radiometer site at each step.

3. Derive the -5 °C isotherm height based on the average heights of the layers above and below the layer equal to -5 °C.

https://doi.org/10.5194/egusphere-2026-4256
Preprint. Discussion started: 19 August 2026

Due to the uncertainties of the radiometer retrievals during rain, the -5 °C isotherm is calculated from 1 h before up to 30 min before the start. If within this time frame all time-steps are flagged by quality control, we consider the time window of 2 h before the event. As a result, for each event we have one value for the -5 °C isotherm, which is the temporal average for the mentioned time-frames.

We label events as 'warm rain' if both the median (over time and space), and the temporal median of the 90th percentile (P90) over space are below the -5 °C isotherm. Similarly, 'cold rain' is selected if both parameters mentioned are above -5 °C isotherm, and 'mixed rain' is when the median is below the -5 °C isotherm, but the temporal median of P90 over space is above the freezing layer. We use the -5 °C isotherm as the reference level for rain type classification, as Korolev et al. (2017) showed that mixed-phase and ice fractions remain small at temperatures warmer than -5, with these fractions increasing substantially only below this threshold. Therefore, echo tops remaining below the -5 °C level are likely dominated by liquid-phase processes (collision-coalescence), while those extending above it increasingly involve ice-phase microphysics processes such as riming. Note that we use the term 'mixed rain' since this classification reflects spatial heterogeneity in echo top heights relative to the -5 °C isotherm. In our framework, mixed rain events are those where the bulk cloud field (identified by median) remains below the -5 °C level, but the deepest cells (identified by P90) extend above it. Throughout the paper, 'warm rain', 'cold rain', and 'mixed rain' refer to these warm-season rain types defined by the echo top relative to the -5 °C isotherm. In particular, 'cold rain' is a warm-season rain type and should not be confused with the separate cold-season category (October to March), which we treat as a single group (see Section 4). Figure 2 shows a flowchart for distinguishing the event regime using echo top and the height of -5 °C.

In order to identify convection, we implemented a radar-based classification scheme as follows: First, we transformed the volume scans onto a Cartesian grid with a maximum height of 10 km, and focused on the period from 2 h before the start of each event to the first 90 min of the event. Then, after preprocessing the data to remove noise and clutter (reflectivity below -20 dBZ, quasi-stationary echoes with radial velocity magnitude $|v_{\mathrm{rad}}|$ below 0.5 m s^{-1}, and correlation coefficient ρ_{hv} below 0.70), we defined four convective criteria, which are evaluated only for meteorological targets where $\rho_{\mathrm{hv}} \geq 0.85$:

- Criterion 1 (high reflectivity structure): Z_{h} exceeds 45 dBZ in the convective core, or is at least 8 dB higher than in the surrounding area, or elevated echoes exceeding 30 dBZ exist 1 km above the freezing level (Steiner et al., 1995).

- Criterion 2 (Z_{DR} column): Z_{DR} values of at least 1 dB extend above the melting layer (Snyder et al., 2015). In addition, mean Z_{DR} above 1.5 dB below the melting layer, indicating size sorting of raindrops by the updraft, increases the score (Zhao et al., 2025).

- Criterion 3 (high specific differential phase K_{DP}): K_{DP} exceeds a threshold of 1.5° km^{-1}, with values between 0.3 and 1.5° km^{-1} contributing partial scores (Bringi and Chandrasekar, 2001).

- Criterion 4 (Doppler velocity v_{rad} and spectrum width w_{rad}): the spectrum width exceeds 4 m s^{-1}, or the local variability of $|v_{\mathrm{rad}}|$ exceeds 10 m s^{-1} (Kim et al., 2021).

https://doi.org/10.5194/egusphere-2026-4256
Preprint. Discussion started: 19 August 2026

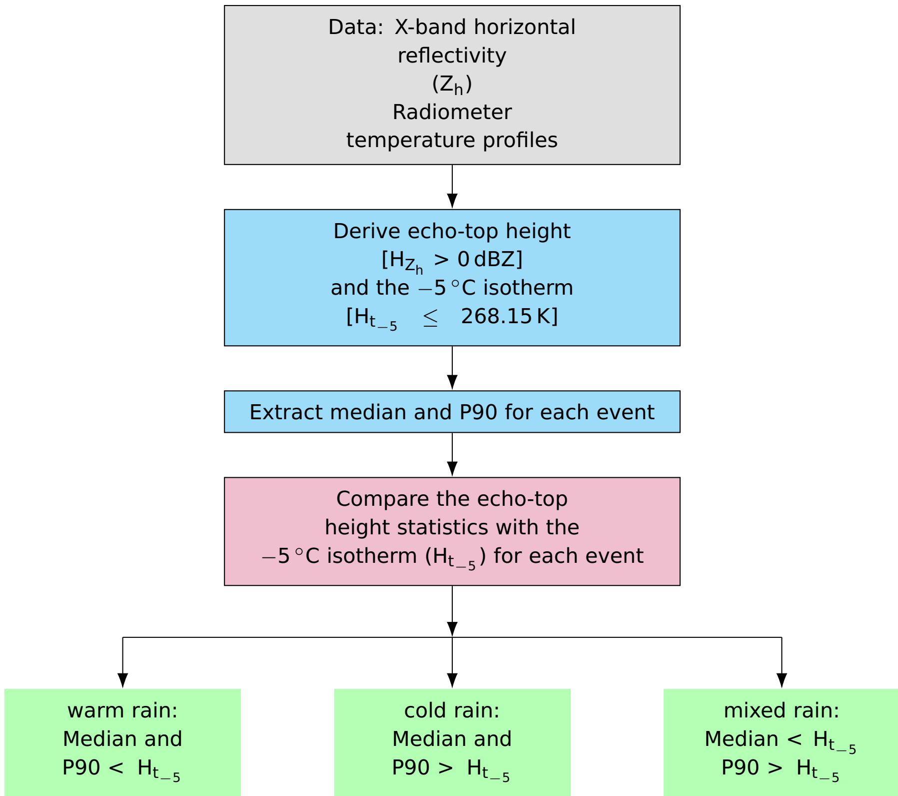

Figure 2. Flowchart for classifying the rain type (warm / cold / mixed) of each event from the radar echo-top statistics (median and P90) relative to the -5 °C isotherm.

Each criterion yields a score between 0 and 1 rather than a strict yes/no decision, and the scores are combined into a convective probability through a weighted sum. Since analyzing hail events is beyond the scope of this study, we calculated a separate hail probability to exclude events where hail occurred from our analysis. For this purpose, a reflectivity higher than 50 dBZ, Z_{DR} between −0.5 and 1.5 dB, and ρ_{hv} between 0.80 and 0.92 are considered (Ryzhkov and Zrnić, 2019; Li et al., 2023). All preprocessing steps and criteria are summarized in Fig. 3.

We calculate these probabilities for each pixel within a 6 km radius around the radiometer site, which is situated at a distance of 14.5 km from the X-band radar. For each rain event, we consider the 95th percentile of the probability calculated above in space for all time steps during that event. Then, the 95th percentile of the time steps are also considered to have one value as the convective probability of that rain event. We define convective as events with convective probability more than 50 %, non-convective (warm season) as events with convective probability less than 50 % that occurred in warm season (April to the end of September), and cold as events that occurred in cold season (October until end of March). Following a sensitivity analysis, different weighting combinations and probability thresholds have impact on the final classification (see Fig. A1). Particularly,

https://doi.org/10.5194/egusphere-2026-4256
Preprint. Discussion started: 19 August 2026

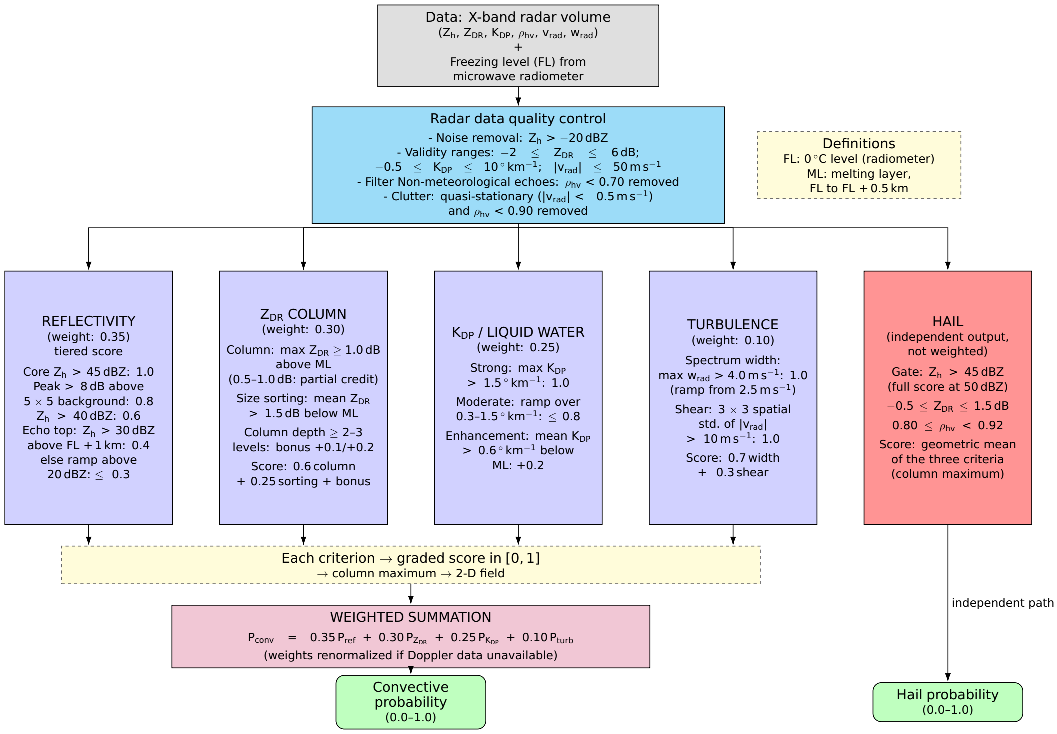

Figure 3. Flowchart of the radar-based convective-probability scheme (warm season): quality control, the four weighted criteria (reflectivity, $Z_{\rm DR}$ columns, $K_{\rm DP}$, turbulence), and the separate hail flag.

the $Z_{\rm DR}$ dominant case shows more convective events, which comes from the processing the radar data and we label it as an artifact (see 11 as an example). Note that we exclude hail events (hail probability more than 50 %) and snow events (using minimum +2 °C 2-m air temperature filter) due to the different hydrometeor characteristics, formation and radar signatures. For each category, we derive LWP, IWV before the precipitation started, as well as 'only cloud' time-steps (defined as times steps that are not within 6 hours before each event until the end of the event).

In addition, we analyzed one event of each cloud precipitation regime as case studies, using different meteorological parameters derived from radar and radiometer data.

4 Results and Discussion

4.1 An overview of LWP and IWV from 2021 to 2025

The monthly changes (median and P90) of the LWP and IWV during these 4 years are shown in Fig. 4 (left). Note that we only used data that are not flagged by quality control and are not interpolated. As seen, IWV has a clear seasonal cycle with sharp changes where maximum and minimum occur in warm and cold seasons, respectively. However, LWP is less sensitive

https://doi.org/10.5194/egusphere-2026-4256
Preprint. Discussion started: 19 August 2026

to seasonal changes compared to IWV. The IWV in warm/cold time-steps has higher values than 'only cloud' time steps, with the difference up to more than 7 kg m^{-2} in some months. For LWP, the difference between warm and cold seasons is generally small, with the 'only cloud' time-steps having low median values (lower than 100 g m^{-2}), and the P90 values for 'only clouds' are also lower than the all-data P90 values. Based on this monthly comparison, the IWV variations are driven more by seasonal differences than by cloud precipitation regime, whereas LWP is more sensitive to precipitating or non-precipitating conditions, with less variation in non-precipitating clouds. It is worth mentioning that we compared monthly LWP and IWV from ERA5 (Hersbach et al., 2020; Hersbach, H. et al., 2023) with the values from microwave radiometer as well (Fig. A2). Overall, the changes in LWP in both datasets are around 20 g m^{-2}, which goes higher in some months. When considering "only cloud" time steps, the differences get higher (about 30 g m^{-2}), with higher values for ERA5 in almost every month (not shown). For IWV, these changes are not noticeable, and both datasets have similar behaviors in each month.

The two panels on the right side of Fig. 4 show the relative-frequency distributions of LWP (top) and IWV (bottom) for the warm-season, cold-season, and no-rain (only-cloud) time-steps. The LWP distribution is strongly right-skewed in all three populations (note the logarithmic axis): most of the values lie at low to moderate LWP, with a long tail towards high values. The warm-season and cold-season distributions are close to each other, and both have higher medians than the no-rain population, so the main separation in LWP is between precipitating and non-precipitating clouds rather than between seasons, similar to the monthly changes. The IWV distribution is clearly separated by season, with a higher warm-season median than the cold-season one, while the no-rain population covers a broad range and overlaps both.

https://doi.org/10.5194/egusphere-2026-4256
Preprint. Discussion started: 19 August 2026

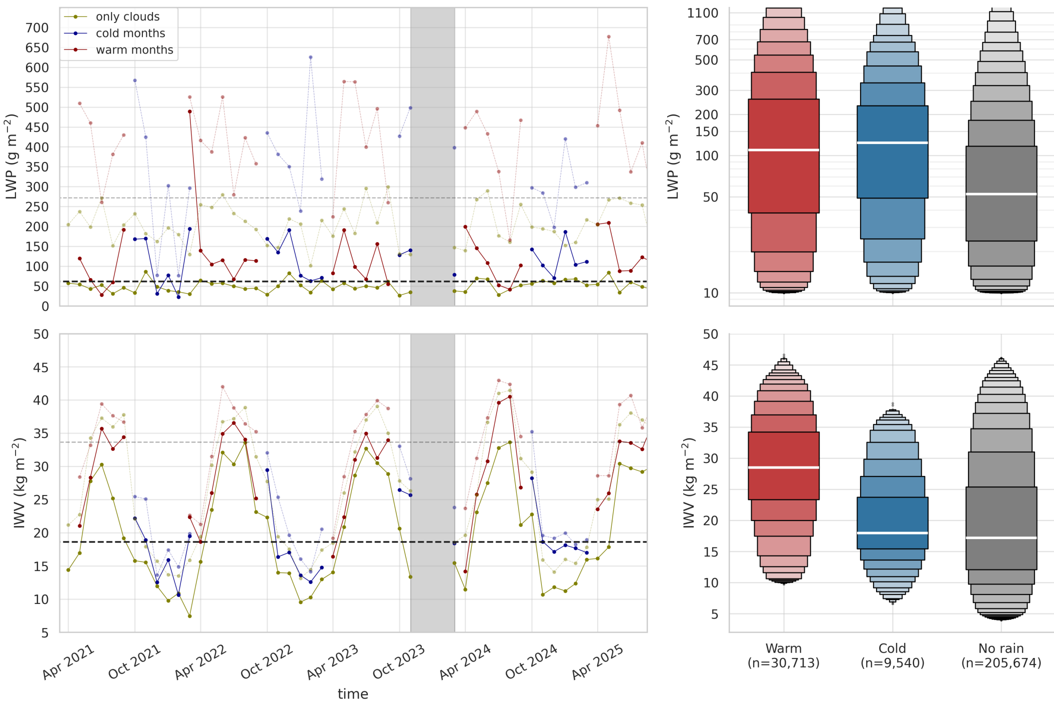

Figure 4. Monthly median (transparent lines) and P90 (semi-transparent lines) and the histogram of liquid water path (top) and IWV (bottom) from 2021 to 2025. The gray zone in the left panels indicates a period where no radiometer data is available. The black dotted horizontal line represents the median of all 'measured' data for both LWP and IWV. The semi transparent shows P90 under the same conditions.

4.2 Changes in LWP and IWV before each precipitation regime

To analyze the parameters before precipitation onset, we considered the 6 h before the event started. There are two reasons for choosing this time-frame: first, our preliminary analysis did not show considerable changes in LWP and IWV earlier than 6 h before onset. Second, different studies have shown that considerable changes in these parameters start within similar or shorter time-frames (e.g. Wang and Hocke (2022); Haas et al. (2025)). Figure 5 shows the changes in LWP up to the start of the rain in different regimes and types. Note that the anomalies are calculated relative to the mean of the values between 6 h and 3 h before onset. As shown, there is a jump in LWP values around 60 min before the rain in all regimes and types, similar to previous studies. Obviously, the results are highly sensitive to the number of valid data points n in each time step, i.e., a lower number causes higher uncertainty. For the convective events, the LWP anomalies are generally smaller up to around 90 min before onset, compared to the other two regimes (non-convective and cold). This could be due to two reasons: first, in convective regimes the cloud development is more local and rapid, so LWP may not build up until very close to onset. Secondly, the microwave radiometer has a limited field of view, so it can only sample the atmosphere within its beam and may miss clouds outside that sampled volume. From 60 min up to onset, a sharp increase in LWP is seen in all regimes, with a steeper slope in the convective events. In the warm rain clouds, rain forms mainly by droplets colliding and merging (collision–coalescence),

https://doi.org/10.5194/egusphere-2026-4256
Preprint. Discussion started: 19 August 2026

which needs liquid water to build up first, which is consistent with the more gradual increase of LWP we see before onset in these clouds (particularly noticeable in warm non-convective rain). This and the higher values of LWP in non-convective warm rain, can be explained by the fact that this type of rain usually comes from larger systems than warm convective rain (shallow convection), which is comparatively more localized. Comparing rain types in convection, cold rain type showed higher LWP close to onset , since these clouds are deeper. The mixed rain type falls between the two warm and cold, as expected, since it contains both deeper cells that reach the ice region and shallower, mostly liquid parts. Note that the warm and mixed convective cases are noisier and based on fewer events, which explains their fluctuations. Note that the LWP values from around 15 min before onset can be unreliable due to the limitations of the radiometer in wet conditions (Cadeddu et al., 2017). That is why these time-steps are shown as hatched and should be interpreted with caution. Furthermore, when interpreting the LWP values in the different rain types (warm, cold, and mixed rain), we should keep in mind that the radiometer cannot see the ice layer above the liquid layer (Vishwakarma et al., 2023).

When considering the absolute values of LWP (Fig. A3), they confirm the low and relatively stable values far from onset, followed by an increase towards the start of the rain, especially in the last hour. Within 30 minutes before start, the warm rain reaches slightly lower LWP values than the cold rain type around 250 g m^{-2}. The instrument effect noted above also matters for interpretation, since in cold-rain cases the radiometer does not capture the ice condensate aloft, so the retrieved LWP reflects liquid water only and should not be read as total condensate. During cold seasons, we consider all events as one category, since having convection during this time is unlikely. In the cold season, LWP begins to increase sharply about 60 min before rain onset, similar to the other categories, although the increase is less intense at around 150 g m^{-2}. Note that the baseline in cold season is higher compared to the warm season, which can be due to pre-existing cloud and/or stratiform cloud regimes.

Similar to LWP, we considered the same time-frame for IWV (Fig. 5). The change in IWV starts earlier compared to LWP, and the IWV absolute values (Fig. A3) in convective events are noticeably higher than the other two regimes (started around 30 kg m^{-2}), as expected due to thermodynamic mechanism as a primary driver. It is worth mentioning that the diurnal cycle confirmed that the number of time-steps for the convective regime (pre-rain time-steps) is higher during 7:00 UTC - 16:00 UTC (not shown), which contributes to the higher values of the IWV in convective regime. This is a sampling effect rather than a purely convective signal, since convective events happen in the warm, moist part of the day, so the convective/non-convective IWV contrast should be interpreted with this diurnal bias in mind. In convective regime, the IWV values increase for all types, with slightly more pronounced increase in warm rain around 3 kg m^{-2} compared to cold rain as cooler, more ice particle column (cold rain) holds less water vapor. The absolute IWV (Fig. A3) can be interpreted with LWP changes in different rain types. In all regimes, IWV is lowest in the cold rain type, in both the convective and non-convective columns. This points to a thermodynamic explanation. Since a cooler column simply holds less water vapor and the saturation vapor pressure rises sharply with temperature (Rogers, 1976), both the water vapor (IWV) and the available liquid (LWP) are lower at the same time. For non-convective clouds, the changes in IWV is slower and less pronounced (with lower absolute values for ice). During cold seasons, the IWV has a gradual increase from 6 hours before the rain starts, and similar to LWP values, less intense compared to the other regimes (up to around 18 kg m^{-2} based on GNSS station). Another difference compare to warm season is that the IWV drops earlier (from -30 min onwards). This may be related to the more widespread and less

https://doi.org/10.5194/egusphere-2026-4256
Preprint. Discussion started: 19 August 2026

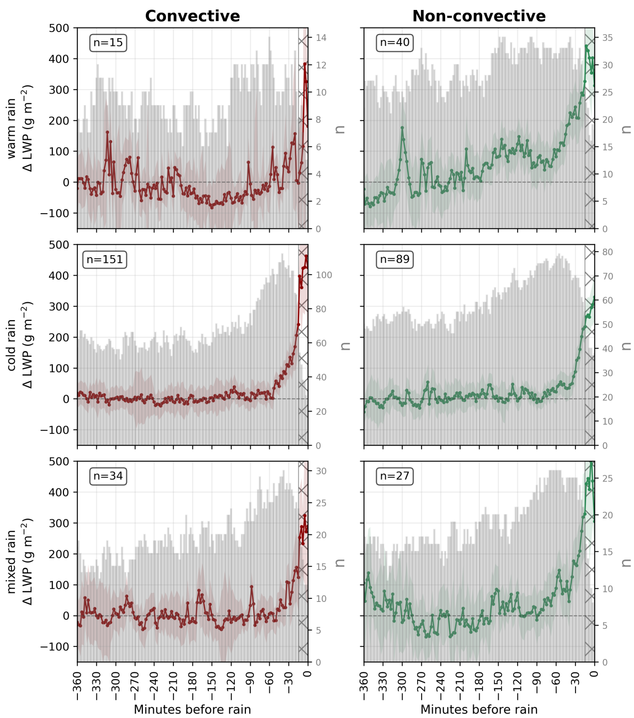

(a) LWP anomalies in warm season in different regimes and types.

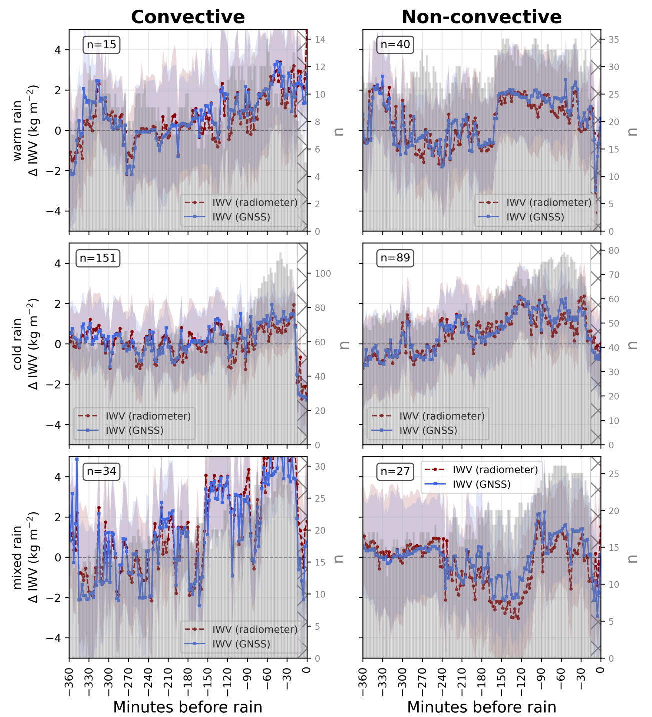

(b) IWV anomalies in warm season

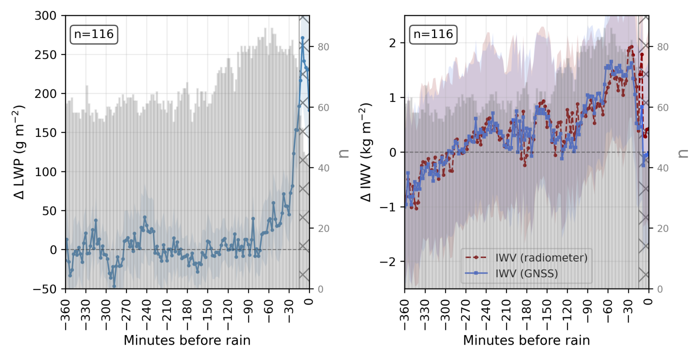

(c) LWP (left) and IWV (right) anomalies in cold season.

Figure 5. Anomalies of (left) LWP and (right) IWV in the warm season, for convective (left sub-columns) and non-convective (right sub-columns) events, split by rain type (warm / cold / mixed, top to bottom). In bottom left, LWP and bottom right , IWV in the cold season are shown. Anomalies are relative to the -6 h to -3 h mean. Shaded bands are 95 % confidence intervals. The last 15 min are hatched to mark the large radiometer uncertainty in wet conditions. The right-hand axis of each panel gives the number of valid events (n).

https://doi.org/10.5194/egusphere-2026-4256
Preprint. Discussion started: 19 August 2026

intense character of cold-season events, where precipitation can already be developing within the larger cloud system before it reaches the station. Additionally, there is a difference from GNSS and the Microwave radiometer in IWV before rain starts in all regimes and seasons, which is on average similar to the previous study by Kvas et al. (2026) with about 1 kg m^{-2} higher in the microwave radiometer retrieval.

To complement the results, we investigate the changes in cloud base height (CBH) derived from the infrared radiometer in different regimes and types as well (Fig. 6). The CBH in convective clouds in all regimes is generally higher with a sharp decrease starting from about -120 min and down by about 1000 m before the start. In non-convective regime, the decrease in CBH starts earlier in warm rain and is milder in cold rain clouds, which can be explained by the same logic as above: first, non-convective systems are more widespread and larger, so the atmosphere has already some cloud, and second the field of view of the radiometer is limited and may miss smaller local systems. We emphasize that, due to the limited number of warm rain events, the uncertainties in this rain type are higher, and this explains the high fluctuations in CBH in this rain type. In cold season, CBH is considerably lower than in warm season (around 1500 m) and started to decrease 60 min before the event by about 300 m, due to colder and moister lower-tropospheric conditions and more persistent low-level or stratiform cloud layers.

https://doi.org/10.5194/egusphere-2026-4256
Preprint. Discussion started: 19 August 2026

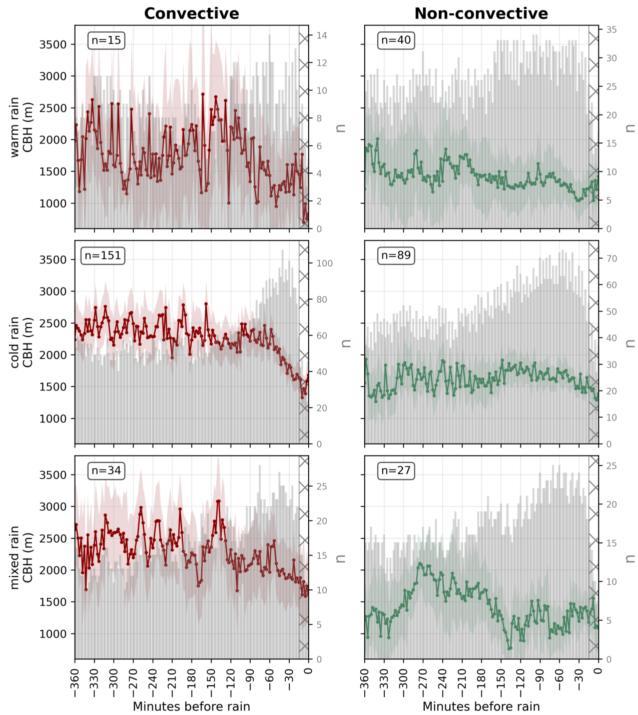

(a) Cloud base height in warm season

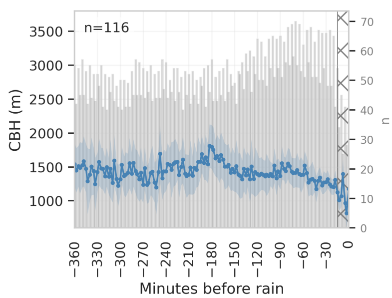

(b) Cloud base height in cold season

Figure 6. Cloud base height before onset, for (top) the warm season (convective and non-convective, by rain type) and (bottom) the cold season. Shaded bands are 95 % confidence intervals. The last 15 min are hatched to mark the large radiometer uncertainty in wet conditions. The right-hand axis gives the number of valid events (n).

https://doi.org/10.5194/egusphere-2026-4256
Preprint. Discussion started: 19 August 2026

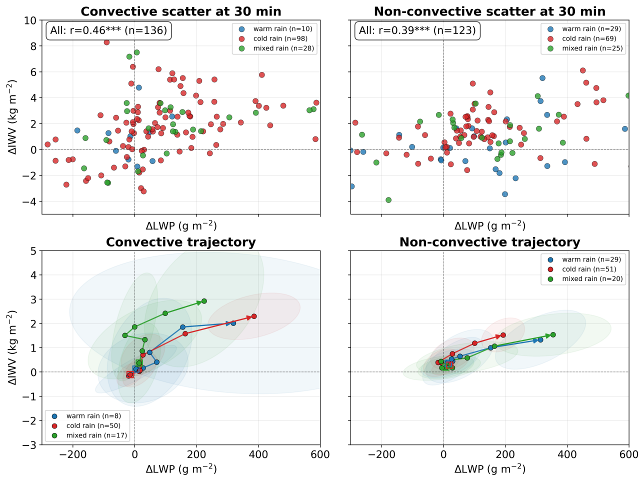

Figure 7. Joint evolution of column moisture and cloud liquid before onset. Snapshot of ΔLWP versus ΔIWV at -30 min, colored by rain type (top), and mean trajectory of ΔIWV versus ΔLWP from -3 h to onset for convective and non-convective events (bottom). Shaded ellipses show the 95% confidence region of the mean position at each time (smaller ellipse = higher certainty).

Figure 7 trajectory figure (bottom) shows IWV (column moisture) and the LWP (cloud liquid) evolve at different rates before the rain. For convective events, the trajectory first moves along the IWV axis (from about -180 to -60 min), indicating that the column moistens before substantial liquid forms. Closer to onset (from about -60 min), the trajectory bends towards higher LWP, transitioning from moisture phase to condensation phase, when updraft partly contributes to the vapor-cloud liquid conversion. Note that the liquid buildup (up to about 0.4 kg m^{-2}) is an order of magnitude smaller than the vapor increase (around 3 kg m^{-2}), so both signals reflect ongoing moisture convergence rather than depletion of column vapor by condensation. For warm and cold rain non-convective events, LWP and IWV increase together along a nearly linear path, with a smaller total moistening, an increase in LWP is consistent with a more gradual, widespread pace, where the liquid builds up in a similar pace with the moisture supply. At the -30 min snapshot, LWP and IWV changes are positively correlated in both regimes (r=0.46 and r=0.39), i.e., events with stronger pre-onset moistening also show stronger liquid buildup. The convective events, however, show a wider spread, which points to their larger event-to-event variability (broader range of updraft strength) compared to the more homogeneous non-convective events, as well as the limitation of the radiometer field of view in more localized events. Note that we checked other time-step (e.g., -20 min and -15 min) for the snapshot plot, which correlation stays positive and of similar strength (not shown). However, the number of the valid points (which is literally the number of valid events at the time), and therefore correlation, change with the chosen time and the wet radome effect near the onset. Moreover, for cold and mixed rain types, the radiometer-derived LWP represents the liquid condensate-only, so the total condensate buildup (including ice) is likely underestimated.

https://doi.org/10.5194/egusphere-2026-4256
Preprint. Discussion started: 19 August 2026

4.3 Case study: a cold convective event on 8 June 2023

This event on 8 June 2023 represents a short, heavy convective precipitation event, which was categorized as a cold convective event (deep convection). On 8 June 2023 during the early afternoon, a small convective cell started to form. The station data show that the event started around 13:30 UTC, and at the peak of the event, 4.3 mm precipitation amount was measured in 5 min. During this event, the temperature fell by almost 10°C, with a sharp increase in peak gust. The radar data show convective activity in the northern part of the station network around 12:45 UTC, with small convective cells. Based on these data, the precipitation peak was 19.2 mm and occurred around 13:47 UTC. This cell moved eastwards, toward the radiometer site, and then started to dissipate.

Figure 8 shows the precipitation amount (left) based on Level 2 radar data (which the reflectivity is already post processed and converted to rain rate), and horizontal reflectivity from the radar (right) over the radiometer site. It also shows cloud base height from the infrared radiometer, LWP, and the -5 °C isotherm from the microwave radiometer. As can be seen, there is a column of high reflectivity (more than 40 dBZ) at the start of the event. The liquid water path started to increase sharply about 20 min before reflectivity appeared over the radiometer site. Note that the LWP value at the last time step before rain onset is flagged and has values higher than 800 g m^{-2}, which is probably related to high brightness temperature values and/or retrieval uncertainties right before rain starts. The cloud base height was around 2 km one hour before the event and decreased to below 1 km before rain onset (similar to long-term analysis). Note that we show the mean cloud base height values over a 20-min window for all case studies to have smoother lines.

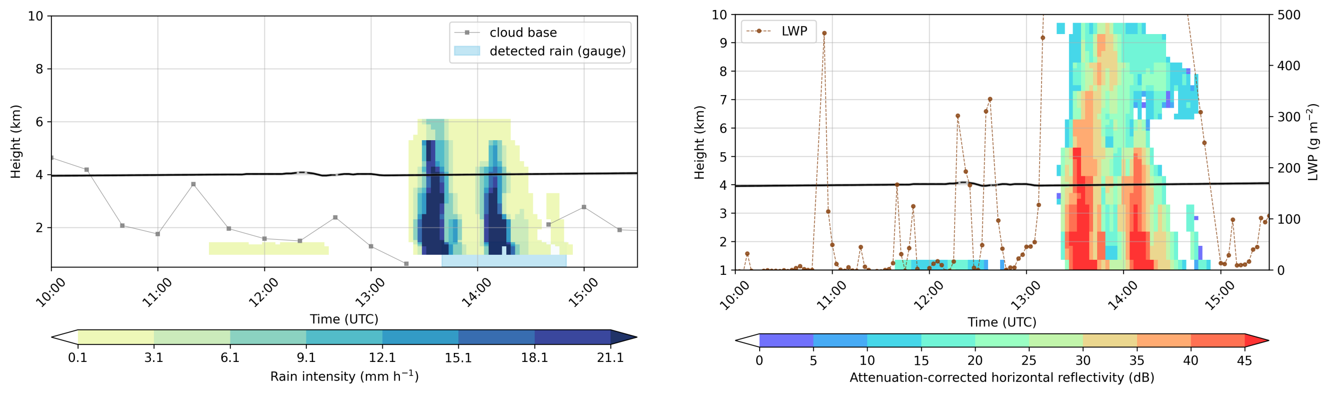

(a) (b)

Figure 8. Precipitation (left) and horizontal reflectivity (right) for the event on 8 June 2023 over the radiometer location detected by X-band radar, LWP is also shown. Note that the black line represents the -5 °C isotherm and gray shade represents the vertical resolution of retrieved temperature (from the radiometer)

Figure 9 shows the differential reflectivity as well as IWV derived from the radiometer for this event. A high Z_{DR} column extending up to about 5 km, together with high reflectivity more than about 1 km above the freezing layer, indicates a strong updraft and liquid drops being lifted into subfreezing levels in this event. Similar to the long-term analysis, IWV increases, but with a higher magnitude of about 4 kg m^{-2}. This case follows the same behavior seen in the long term cold convective events: IWV increases, LWP builds up quickly, and CBH drops sharply before rain onset.

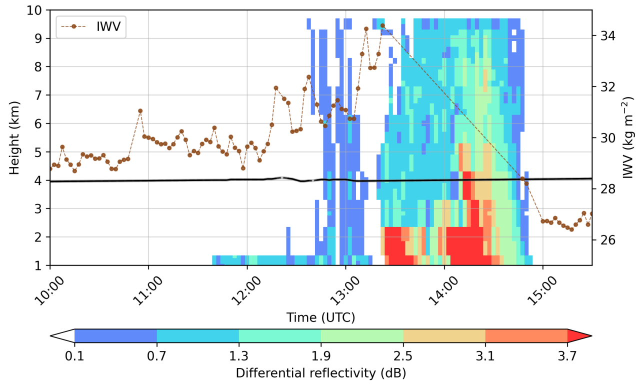

(a)

Figure 9. Differential reflectivity for the event on 8 June 2023 over the radiometer site detected by X-band radar, IWV is also shown

4.4 Case study: a warm convective event on 19 August 2024

Based on the classifications in methodology section, the event on 19 August 2024 falls into the warm convective category. This event was small scale and reached the Feldbach region around 18:15 UTC from the south. Figure 10 shows the precipitation amount based on L2 radar data (left) and horizontal reflectivity (right) over the radiometer site. As seen, the event shows the highest echo around 5.1 km, almost at the -5 °C isotherm. The cloud base height derived from the infrared radiometer shows a noticeable decrease of about 2 km. Moreover, the rise in LWP values is significantly sharp, from 40 g m^{-2} to almost 500 g m^{-2} in the ten-minute steps before the start. Here, the rapid increase in LWP is consistent with long term analysis, which showed the locality of warm convective events (lower LWP earlier, and then sudden jump before the event), and growth of liquid droplets mainly through collision-coalescence.

Figure 11 shows the differential reflectivity as well as IWV derived from the radiometer for this event. Here, in comparison to the previous event, we see lower values of Z_{DR}, indicating smaller drops. Note that the Z_{DR} is extended up to about 9.5 km. Since the horizontal reflectivity is around 5.1 km in the beginning of the events, and the masked ρ_{hv} stops at a similar height (not shown), we interpret this mismatch as an artifact error. Regarding IWV, it shows an increase of about 3 kg m^{-2}. However, the baseline of IWV starts relatively high, because IWV was already around 40 kg m^{-2}, indicating the column was very moist before convection arrived due to another event several hours before. It is worth mentioning, that the echo top is close to the -5 °C isotherm, considering the vertical resolution of the temperature profile. Therefore, the upper part of the cloud may be close to mixed-phase temperatures even if the event is classified as warm rain by the applied method.

https://doi.org/10.5194/egusphere-2026-4256
Preprint. Discussion started: 19 August 2026

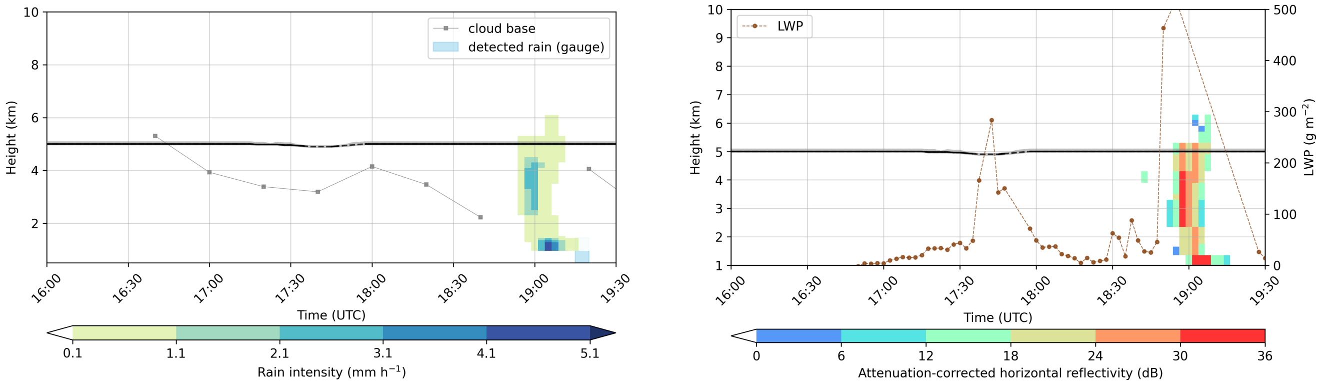

(a) (b)

Figure 10. Precipitation (left) and horizontal reflectivity (right) for the event on 19 August 2024 over the radiometer location detected by X-band radar, LWP is also shown.

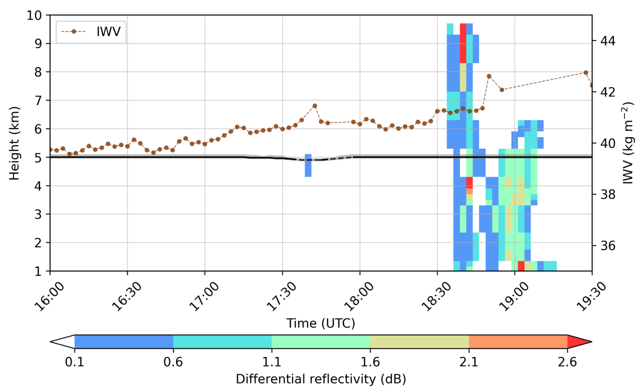

(a)

Figure 11. Differential reflectivity as well as IWV derived from the radiometer for this event. Note that differential reflectivity shows values higher than horizontal reflectivity. which we label as the artifact error.

4.5 Case study: a warm non-convective event on 12 June 2024

Based on the categorization, the event on 12 June 2024 falls into the warm non-convective category. This event was southwesterly and took 1 h and 40 min to exit the Feldbach region. The station measured a temperature around 11 °C and precipitation intensity of about 0.6 mm h^{-1}. The radar estimates precipitation around 07:00 UTC at the radiometer location, when the cloud base height was about 1100 m (Fig. 12). The cloud base height was almost constant before the event and decreased slightly to below 1000 m after the event. Before the event, LWP retrieval was around 300 g m^{-2} at 03:55 UTC. After 05:45 UTC, the radar reflectivity showed about 16 dBZ from the lowest elevation up to 3.2 km above the ground, but two stations farther from the radiometer showed only light precipitation of 0.1 mm h^{-1} during this time. LWP started to rise again from 05:00 UTC and

https://doi.org/10.5194/egusphere-2026-4256
Preprint. Discussion started: 19 August 2026

went up to 400 g m^{-2} 15 min before this event started. The horizontal reflectivity over the radiometer location shows a shallow system with the highest echo a few hundred meters below the -5 °C isotherm.

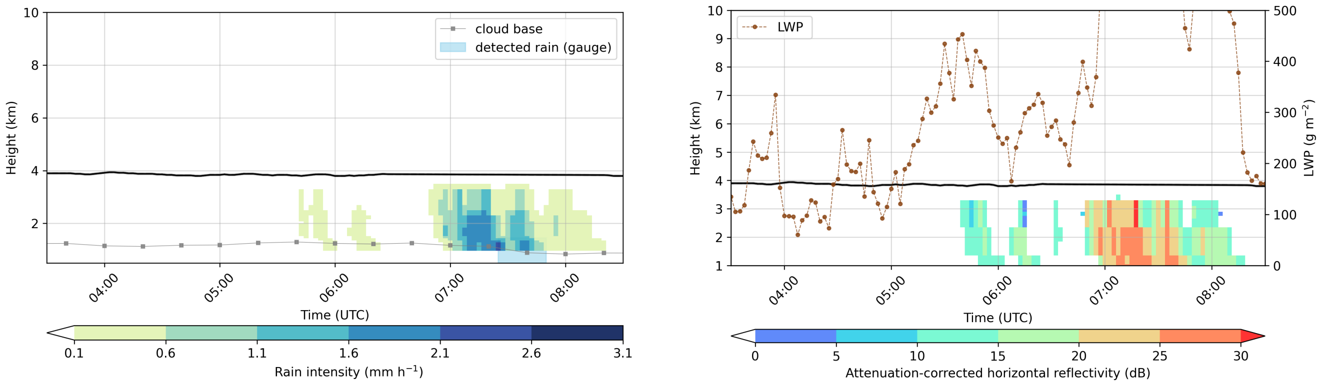

(a) (b)

Figure 12. Precipitation (left) and horizontal reflectivity (right) for the event on 12 June 2024 over the radiometer location detected by X-band radar, LWP is also shown.

315 Figure 13 shows lower Z_{DR}, with a smoother increase in IWV up to about 27 kg m^{-2} before the start. This event shows a different structure compared to the convective events. LWP was already relatively high before the event and then increased more gradually (same pattern for IWV), while CBH stayed near 1 km and changed only slightly. This suggests that the rain development was from an already cloudy lower troposphere rather than from a rapid deepening of the cloud base.

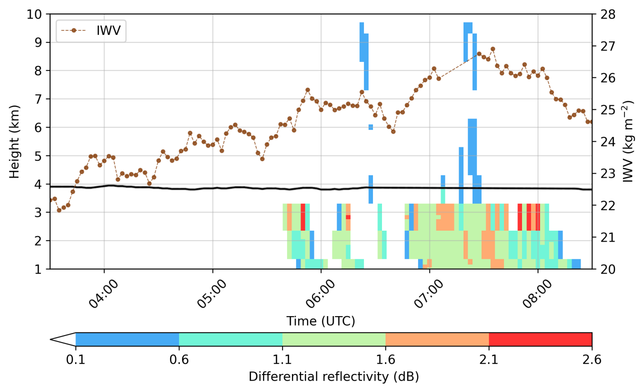

(a)

Figure 13. Differential reflectivity for the event on 12 June 2024 over the radiometer location detected by the X-band radar, IWV is also shown.

https://doi.org/10.5194/egusphere-2026-4256
Preprint. Discussion started: 19 August 2026

5 Conclusions

In this study, we used approximately four years (April 2021–September 2025) of ground-based observations from the WegenerNet 3D Open-Air Laboratory to characterize how liquid water path (LWP), integrated water vapor (IWV), and cloud-base height (CBH) evolve before rain onset across different rain regimes, rain types, and seasons. We separated warm-season events into convective and non-convective regimes using a multi-criteria radar probability scheme, and into warm, cold, and mixed rain types using X-band radar data and temperature profiles from a microwave radiometer. We considered the 6 h before rain onset to examine the changes in each category. Over the four years, IWV followed a clear seasonal cycle, while LWP was more sensitive to whether clouds were precipitating than to the season. This indicates that the two parameters are controlled by different factors: IWV mainly by column temperature and LWP by in-cloud condensate.

Before onset, LWP stayed low and relatively stable far from the event and then increased sharply in all regimes and types, with the steepest increase in convective events reaching about 300 g m^{-2}. The absolute LWP values were lower up to about an hour before rain in convective events (mostly below 80 g m^{-2}) compared with non-convective ones (around 120 g m^{-2} in cold rain), which is consistent with the more local nature of convection, especially in warm rain. Moreover, the rise in LWP started earlier in non-convective events, about 90 min and 120 min before cold and warm rain, respectively. Close to onset, cold-rain events showed somewhat higher LWP than warm-rain events, since clouds are deeper in these types. For IWV, the absolute values in convective events were noticeably higher than in the other two regimes, even at the beginning of the pre-rain period (-6 h): about 32 kg m^{-2} in cold-rain convective events, compared with around 24 kg m^{-2} in cold-rain non-convective events. Additionally, the changes began to appear earlier, around 3 h before rain, with an increase of almost 3 kg m^{-2} in warm-convective rain and about 2 kg m^{-2} in cold rain. When comparing rain types, the absolute IWV values were lowest in the cold-rain type, most clearly in the non-convective regime. Overall, IWV started from a moister column in convective events, while its increase was more gradual and less intense in the larger, more widespread non-convective events. In the cold season, IWV started to rise even earlier, from about 6 h before onset, increasing gradually by about 2 kg m^{-2} and reaching around 19 kg m^{-2} about 30 min before onset, after which it started to decrease.

Moreover, the cloud base decreased before onset in all categories. In convective events, the decrease started roughly 2 h before onset and reached around 1000 m. The decrease was more modest in non-convective events, while in the cold season the cloud base was lower overall and decreased by around 300 m, consistent with rain developing within an already cloudy, near-saturated lower troposphere.

Finally, the changes in LWP and IWV were positively related in both regimes. At 30 min before onset, events with stronger moistening also showed stronger liquid buildup. However, the order of the two signals was not the same. In convective events, the air column first moistened and liquid-water buildup occurred mainly in the last hour, while in non-convective events, liquid water and moisture increased together at a similar pace.

We found general agreement between these findings and other similar studies. For convective events, the results showed changes in LWP, IWV, and CBH before rain similar to those reported by Haas et al. (2025). That study used a different algorithm and focused on convective events selected using the dense gauge network in the region, regardless of rain type. Two

https://doi.org/10.5194/egusphere-2026-4256
Preprint. Discussion started: 19 August 2026

studies over the Swiss Plateau (Wang and Hocke, 2022) and Andalusia, southern Spain (Wang et al., 2024), showed similar signals: IWV had higher absolute values in summer, and it started to increase earlier than liquid water. In Granada, IWV increased by about 5.5 kg m^{-2} during the 6 h before onset, and the integrated liquid water rose from about 40 to 540 g m^{-2} in the last 2 h (Wang et al., 2024), which is a stronger signal than in our study. However, the values are not directly comparable because these studies did not separate their composites by rain type and regime and defined rain onset from the radiometer itself rather than from a gauge. The changes in IWV were also similar to Sapucci et al. (2019) during the CHUVA Vale field campaign in Brazil, with two differences: in their study, the increase in IWV was stronger and occurred closer to rain onset (30 to 60 min). This could be due to differences between the regions, since the CHUVA Vale region is dominated by deep convection (Sapucci et al., 2019). To the authors' knowledge, the pre-rain evolution of LWP, IWV, and CBH has not previously been reported for convective and non-convective regimes together with warm, cold, and mixed rain types. For this reason, the results could only be compared with studies that analyzed the pre-rain evolution without this separation or considered only one of these categories.

These results should be interpreted with several limitations in mind. The radiometer has a limited field of view, and its LWP is unreliable in the last 15 min before onset. Additionally, the warm and mixed convective samples were small and therefore noisier, and the diurnal clustering of convective events contributes to their higher IWV. We also noticed that in some events the echo tops may fall close to the -5 °C isotherm. Considering the vertical resolution of the retrieved temperature profile from the radiometer, these events sit near the classification boundary and therefore their rain type is more uncertain (there is an example in Section 4.4). The radiometer is additionally insensitive to ice, so its LWP should be read as a liquid-only measure rather than total condensate. This mainly affects the cold and mixed rain types, where the total condensate buildup before onset is underestimated. Future work could repeat this analysis in regions with different characteristics (e.g. topography and climate) and use instruments that are also sensitive to ice, so that the total condensate, and not only the liquid part, can be followed.

Overall, the changes in LWP, IWV, and CBH before rain onset differ between the regimes and types, and ground-based remote sensing can capture these signals. The main point is not only that the signals differ in magnitude, but that they occur in a different order. Before convective rain, the column moistens first and liquid-water buildup becomes pronounced mainly in the last hour, while before non-convective rain, moisture and liquid water build up together. This means that the transition from column moistening to cloud-liquid buildup and rain is organized differently depending on the regime, and that a single pre-rain signature is not enough to describe all rain events at one site. In addition, the increase in LWP is nearly an order of magnitude smaller than the increase in IWV (about 0.4 kg m^{-2} versus around 3 kg m^{-2}; Fig. 7). Moreover, until about 30 min before onset in all regimes and types, IWV increases while LWP is already building up, which would not be the case if the column vapor were simply being converted into liquid, so the pre-rain column change is mostly dominated by ongoing moisture supply rather than by depletion of column vapor through condensation. Because these differences appear in parameters that models also produce, they provide an observational target for testing convection-permitting models: not only the magnitude of LWP and IWV before rain, but also their relative timing. Similarly, the regime dependence may be important when these parameters are used as precursors in future nowcasting applications, since similar LWP or IWV changes may have different meanings in convective and non-convective situations.

https://doi.org/10.5194/egusphere-2026-4256
Preprint. Discussion started: 19 August 2026

Data availability. WegenerNet 3D Observing System L1b v1.0 (Kvas et al., 2024a) and L2 v1.0 (Kvas et al., 2024b) X-band radar data, and L2 v8.0 climate station data (Fuchsberger et al., 2025) are available at the WegenerNet Data Portal (https://wegenernet.uni-graz.at/, last access 13 July 2026). Level 2a GNSS and radiometer data Version 2.0-rc1 used are available at https://doi.org/10.5281/zenodo.21350494/, last access 14 July 2026.

https://doi.org/10.5194/egusphere-2026-4256
Preprint. Discussion started: 19 August 2026

Appendix A

A1 Sensitivity analysis for convective classification

Table A1. Different weights in order to calculate sensitivity

Name	weight Z	weight ZDR	weight KDP	weight SW
Baseline	0.35	0.30	0.25	0.10
Z dominant	0.70	0.10	0.10	0.10
ZDR dominant	0.10	0.60	0.20	0.10
KDP dominant	0.10	0.20	0.60	0.10
Reflectivity focus	0.50	0.20	0.20	0.10
Polarimetric focus	0.20	0.35	0.35	0.10
No SW	0.40	0.35	0.25	0.00

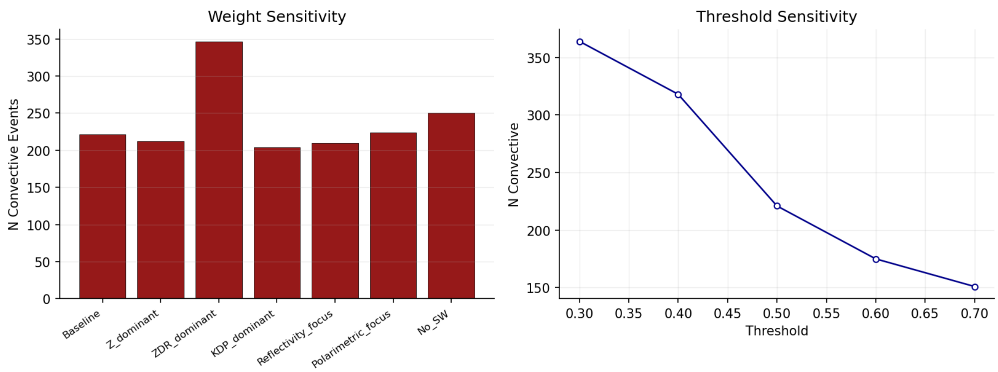

Figure A1. Sensitivity analysis for convective probability weights and thresholds

https://doi.org/10.5194/egusphere-2026-4256
Preprint. Discussion started: 19 August 2026

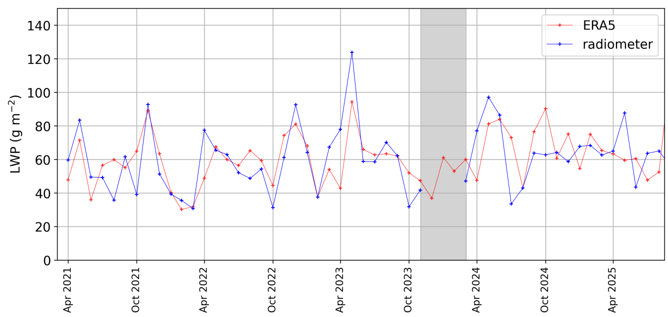

(a) Comparison of LWP monthly changes in ERA5 and microwave radiometer-derived values

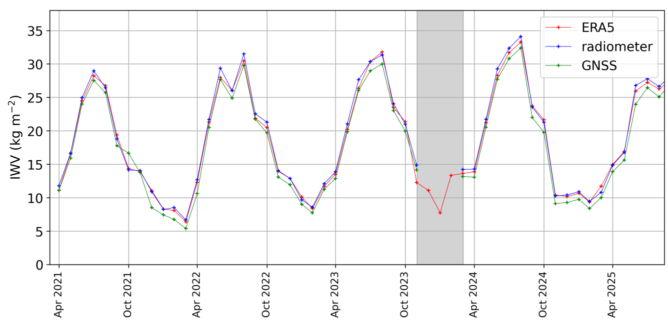

(b) IWV monthly changes in ERA5 and the radiometer

Figure A2. Monthly average and the histogram of liquid water path (top) and IWV (bottom) from 2021 to 2025. The gray zone in the left panels indicates a period where no radiometer data is available.

https://doi.org/10.5194/egusphere-2026-4256
Preprint. Discussion started: 19 August 2026

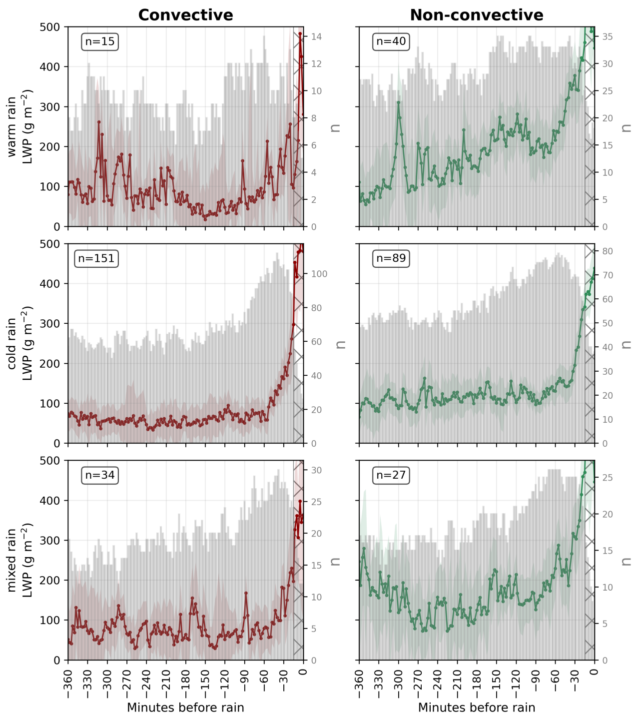

(a) LWP in warm season

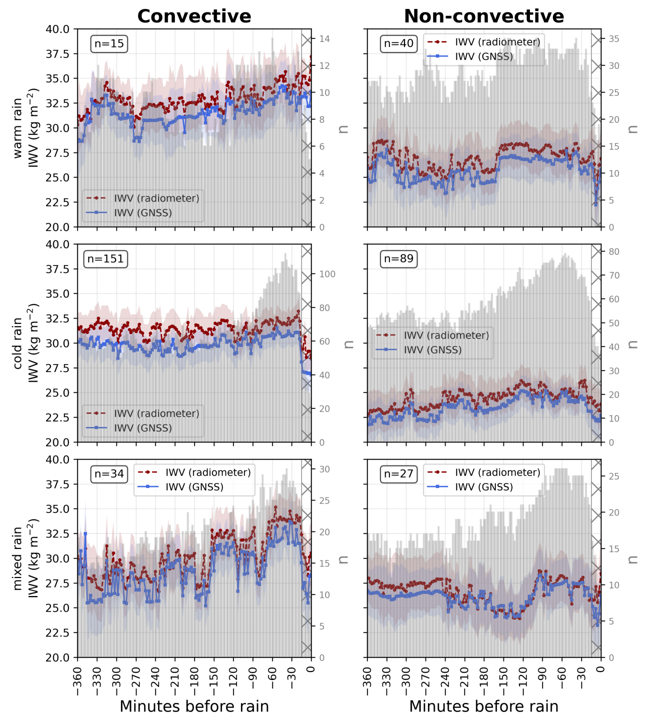

(b) IWV in warm season

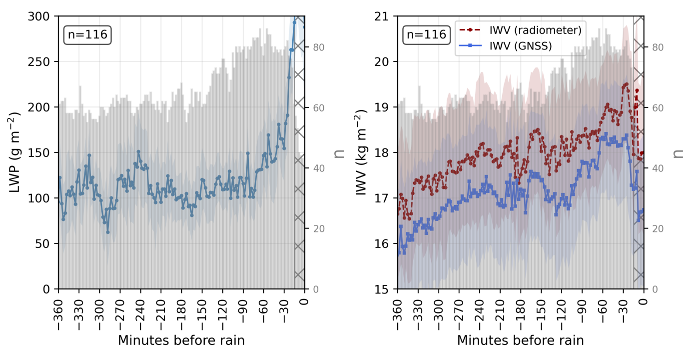

(c) LWP (left) and IWV (right) in cold season

Figure A3. changes in LWP and IWV before starting of the events in different types and regimes. The bands indicate 95% confidence intervals. The last 15 minutes are hatched to indicate the large uncertainty of the radiometer during this period.

https://doi.org/10.5194/egusphere-2026-4256
Preprint. Discussion started: 19 August 2026

A2 Case study: a cold non-convective event on 16 May 2024 (warm season)

We selected one event on 16 May 2024 as a non-convective, cold event to investigate more details regarding the changes in LWP and IWV. This event represents a non-convective event during the warm season in 2024, which started in the late afternoon and continued over the course of the evening. It was a large system that originated from the south and moved northwards, with a maximum intensity of 4.2 mm h^{-1}, and the temperature fluctuated around 15 °C. Figure A4 shows precipitation intensity from Level 2 radar data (left) and horizontal reflectivity. The changes in LWP and cloud base height are shown as well. The radar estimates precipitation around 18:10 UTC, when the cloud base height was about 1200 m. The cloud base height changed within a few hundred meters, considerably less than in the convective regime. Before the event, LWP retrieval had values around 300 g m^{-2} in the afternoon. About 90 min before the event started, LWP started to rise again and went up to 450 g m^{-2} 15 minutes before the start.

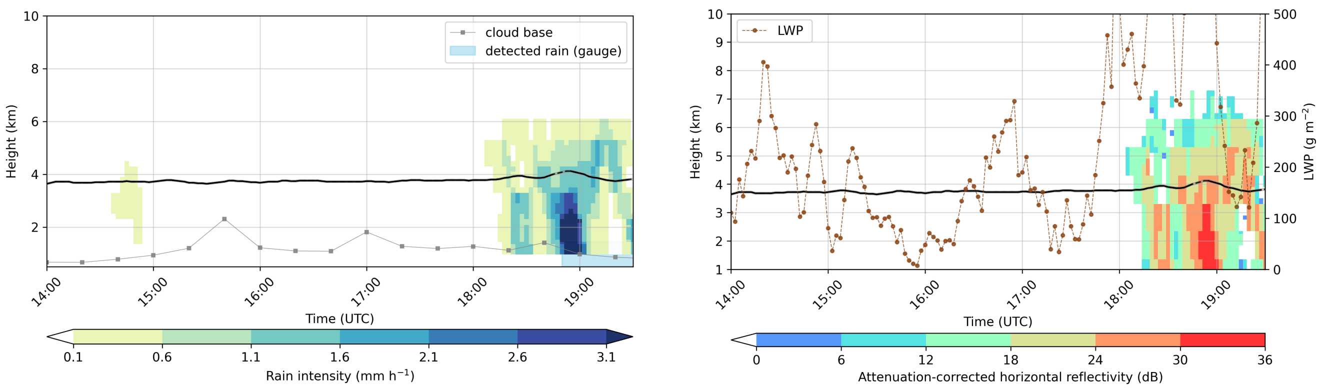

(a) (b)

Figure A4. Precipitation (left) and horizontal reflectivity (right) for the event on 16 May 2024 over the radiometer location detected by X-band radar, LWP is also shown.

The IWV increased from about an hour before the event started and reached almost 29 kg m^{-2} before onset. The relatively small CBH changes indicate that the lower cloud layer was already present and did not deepen as sharply as in the convective cases. This agrees with the long-term non-convective signal: LWP can increase before onset, but CBH changes are weaker.

A3 Case study: a cold season event on 16 March 2025

We investigated one event that occurred during the cold season on 16 March 2025 as an event in the cold season. A westerly system started from 12:10 UTC and lasted until 15:05 UTC. The maximum intensity was 1.3 mm h^{-1} around 13:00 UTC, and the 2-m air temperature was around 6 °C based on climate station data. As can be seen in Figure A6, LWP around 10:00 UTC

https://doi.org/10.5194/egusphere-2026-4256
Preprint. Discussion started: 19 August 2026

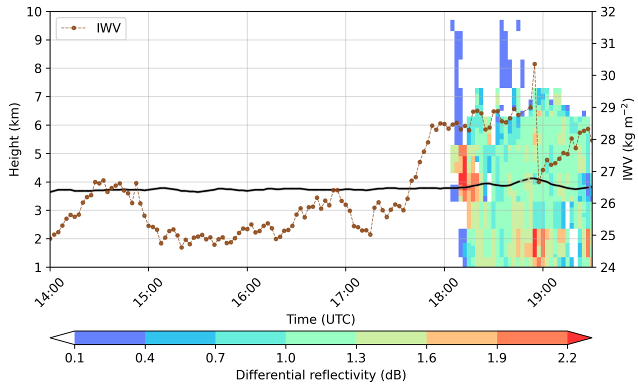

(a)

Figure A5. Differential reflectivity for the event on 16 May 2024 over the radiometer location detected by the X-band radar, IWV is also shown.

starts to rise by about 60 g m^{-2} in about 10 min before the radar starts to report positive reflectivity. Since this is a cold-season case, we should note again that the retrieved LWP does not represent ice condensate aloft. The -5 °C isotherm was around 2.7 km and the cloud base height was very low.

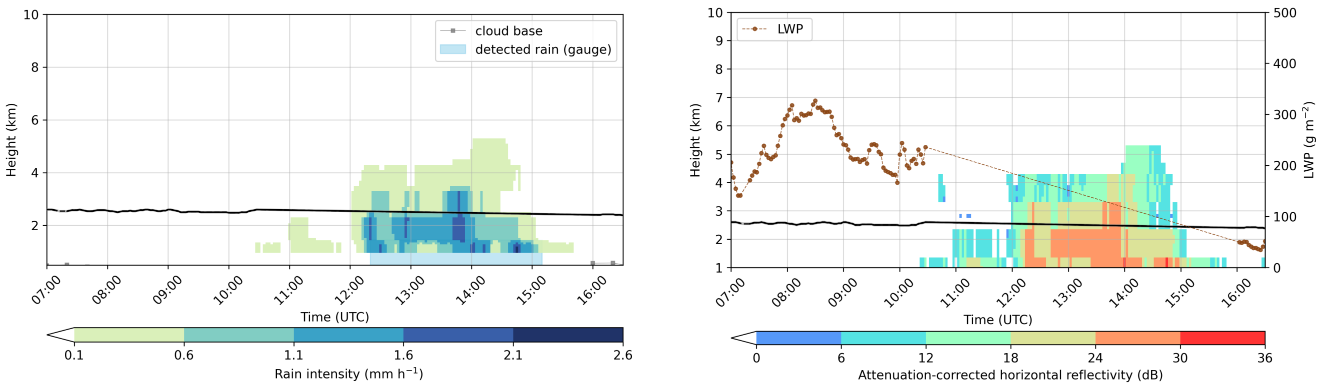

(a) (b)

Figure A6. Precipitation (left) and horizontal reflectivity (right) for the event on 16 March 2025 over the radiometer location detected by the X-band radar, LWP is also shown.

Figure A7 shows Z_{DR} and IWV. The results show that IWV before the event started from about 15 kg m^{-2} and gradually went up to 17 kg m^{-2} before the start. The weak increase of IWV suggests a more moderate moistening of the column compared to the warm-season cases. At the same time, the very low CBH indicates that the lower troposphere was already close to saturation, and the event likely developed in an already cloudy and moist environment. This case supports the interpretation

https://doi.org/10.5194/egusphere-2026-4256
Preprint. Discussion started: 19 August 2026

420 that cold-season precipitation is often connected to a pre-existing cloudy lower troposphere, weaker IWV build-up, and only modest additional liquid-water growth before onset.

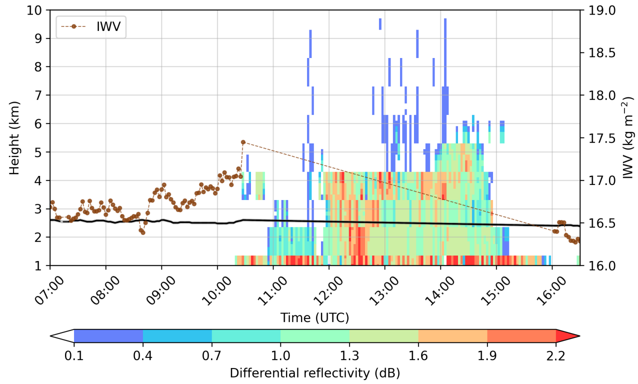

(a)

Figure A7. Differential reflectivity for the event on 16 March 2025 over the radiometer location detected by X-band radar, IWV is also shown.

Author contributions. Conceptualization: EG, PK; Methodology: EG, AK, PK; Formal Analysis: EG, AK; Supervision: UF, PK; Data Curation: AK; Writing – Original Draft: EG; Writing – Review & Editing: EG, AK, UF, PK; Funding acquisition: UF

Competing interests. The authors declare that they have no conflict of interest.

425 *Acknowledgements.* The presented work is conducted under the 'WEGN4CARE' project, funded by Österreichische Forschungsförderungsgesellschaft mbH (FFG), project number FO999911944.

The authors gratefully acknowledge support from NAWI Graz.

This research has been supported by WegenerNet funding that is provided by the Austrian Ministry for Education, Science and Research, the University of Graz, the State of Styria, and the City of Graz; more information can be found online (https://wegcenter.uni-
430 graz.at/en/wegenernet/, last access: 13 July 2026).

The University of Graz also supported the publication costs of the paper.

AI tools were used to support code debugging and commenting, as well as grammar and language checking of the manuscript. All scientific content, analyses, and interpretations are the authors' own, and all text was reviewed, revised, and approved by the authors.

https://doi.org/10.5194/egusphere-2026-4256
Preprint. Discussion started: 19 August 2026

References

Bevis, M., Businger, S., Herring, T. A., Rocken, C., Anthes, R. A., and Ware, R. H.: GPS meteorology: Remote sensing of atmospheric water vapor using the global positioning system, Journal of Geophysical Research: Atmospheres, 97, 15 787–15 801, https://doi.org/10.1029/92JD01517, 1992.

Billault-Roux, A.-C. and Berne, A.: Integrated water vapor and liquid water path retrieval using a single-channel radiometer, Atmospheric Measurement Techniques, 14, 2749–2769, 2021.

Bony, S., Stevens, B., Frierson, D. M., Jakob, C., Kageyama, M., Pincus, R., Shepherd, T. G., Sherwood, S. C., Siebesma, A. P., Sobel, A. H., et al.: Clouds, circulation and climate sensitivity, Nature Geoscience, 8, 261–268, 2015.

Bringi, V. N. and Chandrasekar, V.: Polarimetric Doppler weather radar: principles and applications, Cambridge university press, 2001.

Böck, T., Löffler, M., Marke, T., Pospichal, B., Knist, C., and Löhnert, U.: Instrument uncertainties of network-suitable ground-based microwave radiometers: overview, quantification, and mitigation strategies, Atmospheric Measurement Techniques, 18, 6251–6270, https://doi.org/10.5194/amt-18-6251-2025, 2025.

Cadeddu, M. P., Marchand, R., Orlandi, E., Turner, D. D., and Mech, M.: Microwave passive ground-based retrievals of cloud and rain liquid water path in drizzling clouds: Challenges and possibilities, IEEE Transactions on Geoscience and Remote Sensing, 55, 6468–6481, 2017.

Fuchsberger, J., Kirchengast, G., and Kabas, T.: WegenerNet high-resolution weather and climate data from 2007 to 2020, Earth System Science Data, 13, 1307–1334, 2021.

Fuchsberger, J., Kirchengast, G., and Bichler, C.: WegenerNet climate station network Level 2 data, https://doi.org/10.25364/WEGC/WPS8.0:2025.1, 2025.

Haas, S. J., Kvas, A., and Fuchsberger, J.: Observation based precipitation life cycle analysis of heavy rainfall events in the southeastern Alpine forelands, Weather and Climate Dynamics, 6, 949–963, 2025.

Hersbach, H., Bell, B., Berrisford, P., Hirahara, S., Horányi, A., Muñoz-Sabater, J., Nicolas, J., Peubey, C., Radu, R., Schepers, D., Simmons, A., Soci, C., Abdalla, S., Abellan, X., Balsamo, G., Bechtold, P., Biavati, G., Bidlot, J., Bonavita, M., De Chiara, G., Dahlgren, P., Dee, D., Diamantakis, M., Dragani, R., Flemming, J., Forbes, R., Fuentes, M., Geer, A., Haimberger, L., Healy, S., Hogan, R. J., Hólm, E., Janisková, M., Keeley, S., Laloyaux, P., Lopez, P., Lupu, C., Radnoti, G., de Rosnay, P., Rozum, I., Vamborg, F., Villaume, S., and Thépaut, J.-N.: The ERA5 global reanalysis, Quarterly Journal of the Royal Meteorological Society, 146, 1999–2049, https://doi.org/10.1002/qj.3803, 2020.

Hersbach, H., Bell, B., Berrisford, P., Biavati, G., Horányi, A., Muñoz Sabater, J., Nicolas, J., Peubey, C., Radu, R., Rozum, I., Schepers, D., Simmons, A., Soci, C., Dee, D., and Thépaut, J-N.: ERA5 hourly data on single levels from 1940 to present, https://doi.org/10.24381/CDS.ADBB2D47, 2023.

Kaitna, R., Schlögl, M., Becsi, B., Rieder, H., and Formayer, H.: Climate induced increase in frequency and area affected by critical rainfall conditions triggering debris flows in Austria, Communications Earth & Environment, 6, 793, 2025.

Kim, J.-H., Park, J.-R., Kim, S.-H., Kim, J., Lee, E., Baek, S., and Lee, G.: A detection of convectively induced turbulence using in situ aircraft and radar spectral width data, Remote Sensing, 13, 726, 2021.

Kim, M., Cermak, J., Andersen, H., Fuchs, J., and Stirnberg, R.: A new satellite-based retrieval of low-cloud liquid-water path using machine learning and Meteosat SEVIRI data, Remote Sensing, 12, 3475, 2020.

Kirchengast, G., Kabas, T., Leuprecht, A., Bichler, C., and Truhetz, H.: WegenerNet: A pioneering high-resolution network for monitoring weather and climate, Bulletin of the American Meteorological Society, 95, 227–242, 2014.

Kiszler, T., Ebell, K., and Schemann, V.: A performance baseline for the representation of clouds and humidity in cloud-resolving ICON-LEM simulations in the arctic, Journal of Advances in Modeling Earth Systems, 15, e2022MS003 299, 2023.

Korolev, A., McFarquhar, G., Field, P. R., Franklin, C., Lawson, P., Wang, Z., Williams, E., Abel, S. J., Axisa, D., Borrmann, S., Crosier, J., Fugal, J., Krämer, M., Lohmann, U., Schlenczek, O., Schnaiter, M., and Wendisch, M.: Mixed-Phase Clouds: Progress and Challenges, Meteorological Monographs, 58, 5.1 – 5.50, 2017.

Kvas, A., Fuchsberger, J., Kirchengast, G., and Scheidl, D.: WegenerNet 3D Open-Air Laboratory Level 1b Data, Version 1.0, https://doi.org/10.25364/WEGC/WPS3D-L1B-10, 2024a.

Kvas, A., Fuchsberger, J., Kirchengast, G., and Scheidl, D.: WegenerNet 3D Open-Air Laboratory Level 2 Data, Version 1.0, https://doi.org/10.25364/WEGC/WPS3D-L2-10, 2024b.

Kvas, A., Kirchengast, G., and Fuchsberger, J.: High-resolution atmospheric data cubes from the WegenerNet 3D Open-Air Laboratory for Climate Change Research, Earth System Science Data, 18, 1165–1184, 2026.

Li, N., Zhang, J., Wang, D., and Wang, P.: Research on hail mechanism features based on dual-polarization radar data, Atmosphere, 14, 1827, 2023.

Morrison, H., van Lier-Walqui, M., Fridlind, A. M., Grabowski, W. W., Harrington, J. Y., Hoose, C., Korolev, A., Kumjian, M. R., Milbrandt, J. A., Pawlowska, H., et al.: Confronting the challenge of modeling cloud and precipitation microphysics, Journal of advances in modeling earth systems, 12, e2019MS001 689, 2020.

Niell, A. E.: Global mapping functions for the atmosphere delay at radio wavelengths, Journal of Geophysical Research: Solid Earth, 101, 3227–3246, https://doi.org/10.1029/95JB03048, 1996.

Nissen, K. M., Ulbrich, U., and Leckebusch, G. C.: Vb cyclones and associated rainfall extremes over Central Europe under present day and climate change conditions, Meteorologische Zeitschrift, 22, 649–660, 2013.

Rogers, R. R.: A Short Course in Cloud Physics, Pergamon Press, 1st edn., 1976.

Ryzhkov, A. V. and Zrnić, D. S.: Radar polarimetry for weather observations, vol. 486, Springer, 2019.

Sapucci, L. F., Machado, L. A., de Souza, E. M., and Campos, T. B.: Global P ositioning S ystem precipitable water vapour (GPS-PWV) jumps before intense rain events: A potential application to nowcasting, Meteorological Applications, 26, 49–63, 2019.

Schröer, K. and Kirchengast, G.: Sensitivity of extreme precipitation to temperature: the variability of scaling factors from a regional to local perspective, Climate Dynamics, 50, 3981–3994, 2018.

Skofronick-Jackson, G., Petersen, W. A., Berg, W., Kidd, C., Stocker, E. F., Kirschbaum, D. B., Kakar, R., Braun, S. A., Huffman, G. J., Iguchi, T., et al.: The Global Precipitation Measurement (GPM) mission for science and society, Bulletin of the American Meteorological Society, 98, 1679–1695, 2017.

Snyder, J. C., Ryzhkov, A. V., Kumjian, M. R., Khain, A. P., and Picca, J.: A Z DR column detection algorithm to examine convective storm updrafts, Weather and Forecasting, 30, 1819–1844, 2015.

Steiner, M., Houze Jr, R. A., and Yuter, S. E.: Climatological characterization of three-dimensional storm structure from operational radar and rain gauge data, Journal of Applied Meteorology and Climatology, 34, 1978–2007, 1995.

Stevens, B. and Bony, S.: What are climate models missing?, science, 340, 1053–1054, 2013.

Vishwakarma, P., Delanoë, J., Jorquera, S., Martinet, P., Burnet, F., Bell, A., and Dupont, J.-C.: Climatology of estimated liquid water content and scaling factor for warm clouds using radar–microwave radiometer synergy, Atmospheric Measurement Techniques, 16, 1211–1237, 2023.

https://doi.org/10.5194/egusphere-2026-4256
Preprint. Discussion started: 19 August 2026

Walbröl, A., Crewell, S., Engelmann, R., Orlandi, E., Griesche, H., Radenz, M., Hofer, J., Althausen, D., Maturilli, M., and Ebell, K.: Atmospheric temperature, water vapour and liquid water path from two microwave radiometers during MOSAiC, Scientific Data, 9, 534, 2022.

Wallace, J. M. and Hobbs, P. V.: Atmospheric science: an introductory survey, vol. 92, Elsevier, 2006.

Wang, W. and Hocke, K.: Atmospheric effects and precursors of rainfall over the Swiss Plateau, Remote sensing, 14, 2938, 2022.

Wang, W., Hocke, K., Nania, L., Cazorla, A., Titos, G., Matthey, R., Alados-Arboledas, L., Millares, A., and Navas-Guzmán, F.: Interrelations of precipitation, aerosols, and clouds over Andalusia, southern Spain, revealed by the Andalusian Global ObseRvatory of the Atmosphere (AGORA), Atmospheric Chemistry and Physics, 24, 1571–1585, 2024.

Wang, Z., Wang, Z., Cao, X., Mao, J., Tao, F., and Hu, S.: Cloud-base height derived from a ground-based infrared sensor and a comparison with a collocated cloud radar, Journal of Atmospheric and Oceanic Technology, 35, 689–704, 2018.

Xi, B., Dong, X., Zheng, X., and Wu, P.: Cloud properties over the Southern Ocean during the MARCUS field campaign, Atmospheric Measurement Techniques Discussions, pp. 1–44, 2022.

Zhao, C., Zhang, Y., Zhai, H., Li, Z., Zheng, D., Peng, X., Yao, W., Du, S., and Du, Y.: Bridging the polarimetric structure and lightning activity of isolated thunderstorm cells during the cloud life cycle, Atmospheric Chemistry and Physics, 25, 13 453–13 473, 2025.